Cement and Concrete Research 40 (2010) 1734–1743

Contents lists available at ScienceDirect

Cement and Concrete Research

journal homepage: http://ees.elsevier.com/CEMCON/default.asp

Non-destructive evaluation of concrete using a capacitive imaging technique: Preliminary modelling and experiments

X. Yin [a], D.A. Hutchins [a], G.G. Diamond [a], P. Purnell [b,*]

[a] School of Engineering, University of Warwick, Coventry CV4 7AL, UK
[b] School of Civil Engineering, University of Leeds, Leeds LS2 9JT, UK

ARTICLE INFO

Article history:
Received 16 March 2010
Accepted 23 August 2010

Keywords:
Crack detection (B)
Electrical properties (C)
Reinforcement (D)
Modelling (E)
Non-destructive evaluation

ABSTRACT

This paper describes the application of capacitive imaging to the inspection of concrete. A two-dimensional finite-element method was employed to model the electric field distribution from capacitive imaging probe, and how it interacts with concrete samples. Physical experiments with prototype capacitive imaging probes were also carried out. The proof-of-concept results indicated that the capacitive imaging technique could be used to detect cracks on the surface of concrete samples, as well as sub-surface air voids and steel reinforcement bars.

1. Introduction

Reinforced concrete is one of the most important construction materials because it is economical, durable and has the ability to be cast into any shape. In most cases reinforced concrete is reliable and strong throughout its service life. However, factors such as poor design, bad workmanship and a harsh environment can combine to cause deterioration within a concrete structure. This may induce failure of the structure by causing visually unacceptable surface cracking or spalling of the layer of concrete 'cover' that protects the steel reinforcement. This may in turn pose a safety risk to passing pedestrian or motor traffic owing to falling debris, and ultimately lead to further corrosion and structural failure. Unfortunately, more often than not, this deterioration may not become apparent at the surface until major damage has already occurred. Similarly, in assessing heritage concrete structures, poor record keeping may prevent an accurate knowledge of the quantity and architecture of the internal steel reinforcement being known in advance. Thus non-destructive evaluation (NDE) techniques are very useful for condition assessment of concrete structures, so as to provide information concerning structural conditions within the material. These include:

- cracks caused by shrinkage of concrete or repetitive freeze–thaw cycles;
- corrosion of reinforcing steel caused by an ingress of chloride ions (e.g. from sea water or de-icing salt) and/or loss of steel passivity owing to neutralization of the normal alkaline environment provided by the concrete cover by reaction with atmospheric carbon dioxide;
- weak areas of concrete and/or discrete defects caused by poor quality control in the mixing and placing of concrete (*e.g.* poor curing, incorrect mix design, air voids *etc.*);
- the size, depth and distribution of steel reinforcement bars (rebars) and their condition with respect to corrosion *etc.*

There is a range of techniques used conventionally to inspect concrete structures. They are all designed to detect only a single type of artefact (e.g. rebar, void, corrosion etc). Perhaps the most common is the covermeter [1]. This operates by creating eddy currents within the rebars, and measuring the resultant magnetic field at the concrete surface to gain diagnostic information. This approach is used to estimate cover depth and to give some idea of rebar position, but is difficult to use beyond a certain cover depth or in areas of congested reinforcement and does not easily provide an imaging capability [2]. Ultrasonic techniques are also used to assess concrete structures, using various transducer technologies and frequencies, including relatively simple, low-frequency piezoelectric systems such as the PUNDIT™ [3], more advanced piezoelectric transducer designs [4–6] and the use of air-coupling [7,8]. However, this approach has yet to receive widespread use for rebar and void characterization because of uncertainties introduced by the significant ultrasonic scattering encountered [9,10], which is a manifestation of the mismatch in acoustic impedance between aggregates, cement paste matrix and non-critical small air voids being of similar magnitude to that between concrete and voids or rebars. In many cases, surface preparation is also required.

* Corresponding author.
E-mail address: P.Purnell@leeds.ac.uk (P. Purnell).

0008-8846/$ – see front matter © 2010 Elsevier Ltd. All rights reserved.
doi:10.1016/j.cemconres.2010.08.015

The half-cell potentiometer can be used to infer the probability of corrosion of the steel rebar from the surface of the concrete [11,12] by measuring the electrochemical potential between the rebars and a reference 'half-cell' electrode at the surface. Areas of high potential gradient are more likely to be undergoing corrosion. This approach must be combined with other techniques (e.g. resistivity surveys) in order to obtain quantitative results. It sometimes also requires a complicated statistical analysis to retrieve useful data [13] or to predict service life [14]. It also requires that an electrical connection be made to the rebar, which normally entails breaking or cutting out a section of cover concrete. Ground Penetrating Radar (GPR) has also been proposed for the inspection of concrete structures [15,16]. The resolution of GPR system is limited to 100 mm for commercial systems owing to the wavelength used [17,18] which is not really suitable for the majority of artefacts of interest in structural assessment. Other electromagnetic techniques, such as electrical resistance measurement [19,20], impedance spectroscopy [21] and electrical resistance tomography [22] are reported to be used for inspection and evaluation of concrete structures, but they all require a perfect electrical contact between the electrode and the target surface.

The capacitive imaging approach described in this paper aims to offer a possible route to overcoming some of the limitations imposed by existing NDE techniques on the inspection of concrete structures. For example, the technique should be able to recognize both rebars and air voids within a concrete structure. Since our first demonstration of 'proof of concept' for capacitive NDE with concrete [23], other work has described capacitive approaches to measure cover depth and water content, in conjunction with GPR [24]. The technique has also been used for detecting water intrusion in composite structures [25], and for inspecting laminated composite plates [26].

Here, the technique is investigated in some depth to further evaluate its possible application to concrete structures. This paper describes the results from both finite element modelling and physical experiments to investigate the usefulness of the capacitive technique for concrete inspection and imaging. It follows on from previous papers [27,28], where preliminary experiments on a wide range of materials were described. It should be noted that the intention is to demonstrate the potential of capacitive techniques to, in principle, detect artefacts within concrete samples. Thus, the artificial artefacts introduced in the samples, and the conditions under which they were tested, were designed to provide clear results rather than exactly simulate in-service situations. We discuss the concomitant limitations in section 5.

2. Apparatus

The general approach adopted during this work was to use a co-planar capacitive electrode to detect changes in the local electrical characteristics within a concrete sample. Fig. 1 shows schematically how the electric field shapes vary as the two electrodes of a capacitor change from a parallel-plate geometry to being co-planar, so that a fringing field is produced. It is this fringing field that extends into the concrete sample for imaging purposes, with the concrete effectively acting as the dielectric within the capacitor. Scanning such an electrode pair across a surface and measuring the resultant change in stored charge for a given voltage would then create a map of changes in electrical properties within the concrete.

A schematic diagram of the capacitive imaging approach is shown in Fig. 2. The co-planar probe, which contains two or more metal electrodes, generates an electric field distribution within the test material when an AC voltage is applied between the positive and negative electrodes. The presence of the sample under test will affect the resultant electric field pattern, and furthermore, any property change in the sample (such as the presence of a defect) within the volume covered by the electric field distribution will also have an effect, as shown in Fig. 2. The resultant electric field distortion will then result in a change in the charge induced at the sensing electrode, and this change in signal can be detected and used for imaging purposes. Since concrete, water, steel rebar and air voids/cracks all have very different electric properties, the electric field distribution is affected differently by these areas within the sample, giving a basis for imaging.

Note that this approach is a non-contact technique and the air gap between the electrodes and the sample can be quite large (on the order of millimetres). Thus, sample surface preparation is often not required. In addition, the approach only requires single-sided access to the test sample.

A typical capacitive imaging probe is shown in Fig. 3. The co-planar triangular imaging electrodes, plus the grounded guard electrodes (used for shielding the two electrodes electrically from each other) are fabricated by etching a printed circuit board (PCB) substrate. The PCB was also coated in copper on its rear surface and mounted in a metal box to shield the electrodes from electrical noise interference, and to enhance the radiated electric field magnitude in the direction of the sample surface. For an accurate evaluation of concrete, the electrode geometry must be designed with some care. Sensors of various geometries have been investigated in previous work [28], and the results have indicated that it is important to optimise the electrode geometry for each application. Generally, a wider electrode assembly will provide a deeper depth of penetration into the sample, but this will be traded off against a reduced spatial resolution at the surface. In this work, experimental results were obtained using triangular electrodes such as those shown in Fig. 3, but with different sizes to suit each application.

The probe was part of an instrumentation system that could be used for imaging, and a schematic diagram of the basic instrumentation is shown in Fig. 4. To measure the signal at any particular location, a single frequency AC signal was applied as the driving voltage to one of the electrodes. The frequency of operation could be adjusted from 10 kHz to 1 MHz. Note that all the images present in this paper were obtained at a frequency of 1 MHz, unless stated otherwise. The drive voltage waveform was obtained from a Turlby Thandar Instruments TG120 signal generator. The capacitance across the electrodes was not measured directly, as this would not be sufficiently sensitive. Instead, a Cooknell CA/6 charge amplifier was used to convert the charge signal on the sensing electrode to an AC

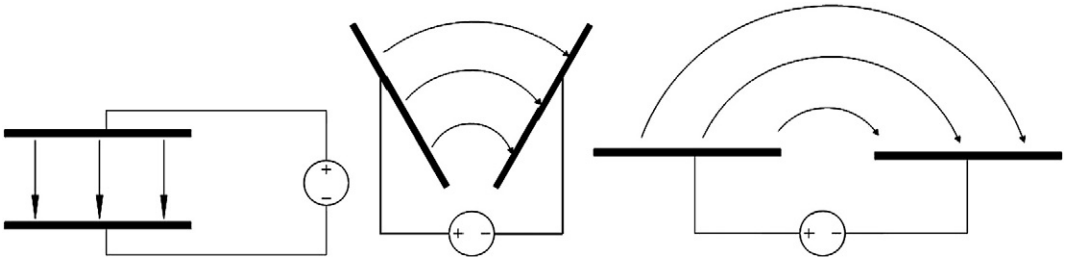

Fig. 1. Schematic diagram of the electric field distribution as electrodes change from being in a conventional parallel-plate capacitor geometry (left) to become co-planar (right).

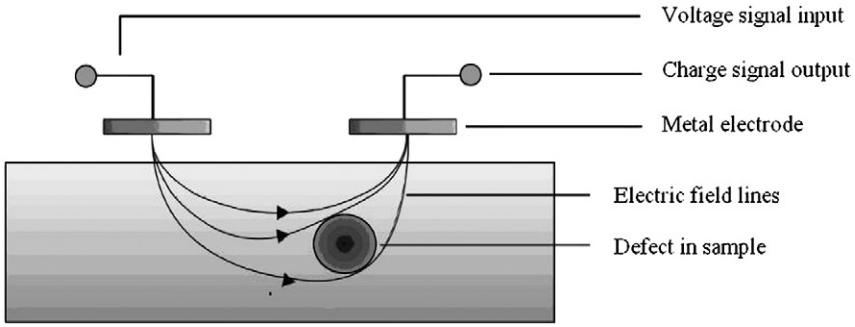

Fig. 2. Schematic diagram of the capacitive imaging approach.

voltage signal, which could then be recorded if desired. However, greater sensitivity was obtained by using a Scitec 441 lock-in amplifier, which converts the AC voltage signal into a DC voltage proportional to the amplitude of the received AC signal. The lock-in amplifier is an example of phase-sensitive detection, and allows a high degree of noise suppression in small signal measurements such as these. The DC output was then recorded using a Tektronics TDS 430 oscilloscope, and transferred to the PC for storage. The PC also controlled an X–Y scanning stage, which could be used to translate the capacitive imaging electrodes across the sample surface, and the signal recorded in specified locations so as to build up an image.

3. Two-dimensional finite element (FE) modelling

In order to understand the way in which electric field distributions are produced by the electrodes, and to indicate how they may interact with the materials of interest, it was felt important to model the expected behaviour. Techniques such as conformal mapping [29] can be used to calculate the capacitance of a planar capacitor electrode assembly, but in the present work we are more interested in the distribution of the electric field and how changes within the sample might affect the capacitance. Finite element (FE) modelling [28,30] has thus is been employed to predict the fields from capacitive electrodes and to predict the changes in signal that were likely to be produced under experimental conditions.

Fundamentally, the electromagnetic phenomena are governed by the Maxwell's equations. In a general case of materials exhibiting both dielectric and conductive properties, such as concrete, the Maxwell–Ampere equation is considered.

$$\nabla \times \boldsymbol{H} = \boldsymbol{J} + \frac{\partial \boldsymbol{D}}{\partial t} \tag{1}$$

where $\boldsymbol{H}$ is the magnetic field intensity, $\boldsymbol{J}$ is the free current density and $\boldsymbol{D}$ is the electric flux density. To eliminate the magnetic field intensity $\boldsymbol{H}$, the divergence of both sides of Eq. (1) is taken, as:

$$\nabla \bullet \left(\boldsymbol{J} + \frac{\partial \boldsymbol{D}}{\partial t} \right) = 0 \tag{2}$$

The frequencies used in capacitive imaging probes are generally in the region between 10 kHz and 1 MHz. At such frequencies, inductive phenomena can be neglected and the electromagnetic field can be considered as a quasi-static electric field. It can then be assumed that the time-derivative of the magnetic flux density ($\boldsymbol{B}$) is negligible, and based on Faraday's Law the electric field ($\boldsymbol{E}$) is curl free,

$$\nabla \times \boldsymbol{E} = -\frac{\partial \boldsymbol{B}}{\partial t} = 0 \tag{3}$$

Based on Eq. (3), the electric field ($\boldsymbol{E}$) can be described by an electric scalar potential distribution $\varphi(x, y, z)$, so the electric potential distribution $\varphi(x, y, z)$ can be introduced as

$$\boldsymbol{E} = -\nabla \varphi(x, y, z) \tag{4}$$

and using the constitutive relationships

$$\boldsymbol{J} = \sigma(x, y, z)\boldsymbol{E} \tag{5}$$

$$\boldsymbol{D} = \varepsilon(x, y, z)\boldsymbol{E} \tag{6}$$

Eq. (2) can take the form

$$\nabla \bullet [\sigma(x, y, z)\nabla \varphi(x, y, z)] + \nabla \bullet \left\{ \frac{\partial}{\partial t} [\varepsilon(x, y, z)\nabla \varphi(x, y, z)] \right\} = 0 \tag{7}$$

Here, $\sigma(x,y,z)$ is the conductivity distribution and $\varepsilon(x,y,z)$ is the permittivity distribution. If the conductivity and permittivity distributions within the area of interest covered by the electric field are known, the electric potential distribution $\varphi(x,y,z)$ can be obtained by solving Eq.(7). But in practice, due to the time-derivative coupling between the dielectric and conductive properties, solving Eq.(7) is computationally prohibitive [30]. The practical way of solving this problem is to treat the system as either "predominantly dielectric" or "predominantly conductive" [30]. In the former case, Eq. (7) can be simplified to be:

$$\nabla \bullet [\varepsilon(x, y, z)\nabla \varphi(x, y, z)] = 0 \tag{8}$$

This equation is valid, for example, for Electrical Capacitance Tomography (ECT) applications [31,32] and dielectrometry sensors [26]. In the latter case, the equation becomes

$$\nabla \bullet [\sigma(x, y, z)\nabla \varphi(x, y, z)] = 0 \tag{9}$$

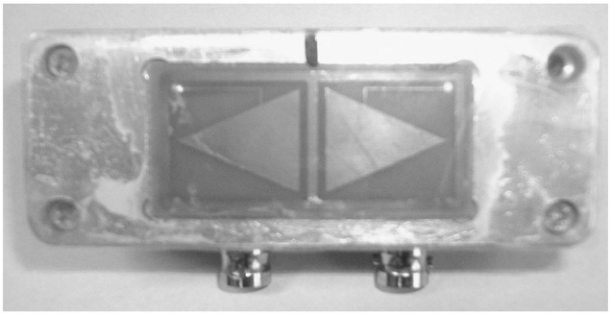

Fig. 3. Photograph of a pair of triangular electrodes, mounted in a shielded metallic container. The triangular electrodes in this example were each 20 mm wide in the horizontal direction.

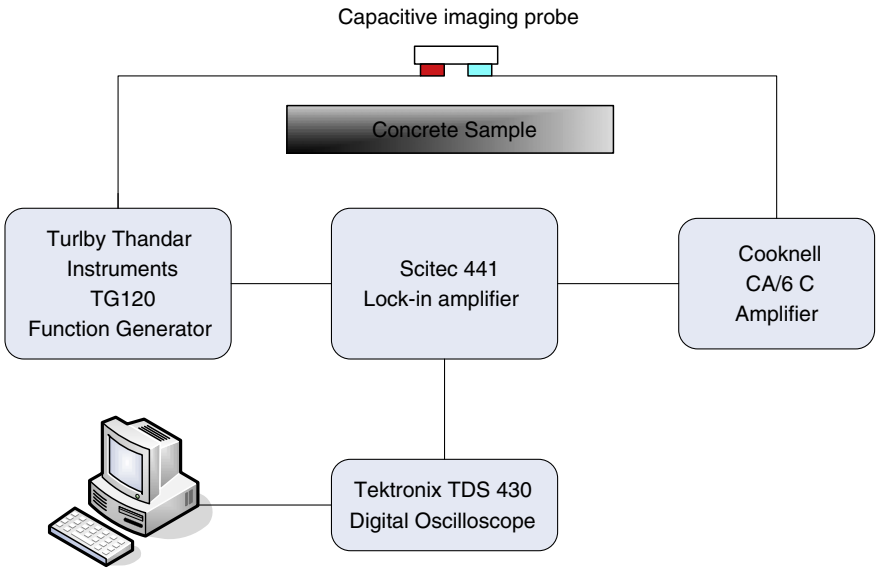

Fig. 4. System block diagram of capacitive imaging system.

which is valid for Electrical Resistance Tomography (ERT) applications [22,33,34] and potential drop methods [35,36].

Using the quasi-static assumption mentioned above, it is possible to use a finite element (FE) technique to solve the above equations, and to predict the potential distribution $\varphi(x, y, z)$ produced by the capacitive electrodes in a particular medium and geometry. In addition, Gauss's Law in a numerical integral form can be applied on the surface enclosing the sensing electrode to calculate the induced charge on that electrode that would result from that electric potential distribution if desired. Gauss's Law can be written as:

$$q = -\oint_{s} \varepsilon(x,y,z)\nabla\varphi(x,y,z)d\boldsymbol{s} \tag{10}$$

where $\boldsymbol{s}$ is the surface enclosing the sensing electrode.

It can be shown by an analysis of Eqs. (7)–(10) that, for a given driving signal, the amount of charge on the sensing electrode is solely determined by the electrical properties of the materials within the field (via the permittivity and conductivity distributions $\varepsilon(x, y, z)$ and $\sigma(x, y, z)$ respectively). Thus, changes of structure or material within a concrete structure which change the permittivity and conductivity distributions will change the total charge on the sensing electrode, which can then be represented as a variation in the final image. It will be shown later in this paper that the capacitive technique is capable of imaging both cracks on the surface and sub-surface air voids, whilst simultaneously being able to locate rebar within concrete specimens.

Theoretical simulation models were constructed using the COMSOL™ Multiphysics FE package (version 3.3), which can be used to model the predictions of such equations for different geometries. To simplify the models, simulations were restricted to two dimensions. The quasi-static model was used within COMSOL, in which it is assumed that the electric field is not propagating along the electrodes, and that there is no coupling between the electric and magnetic fields. In this model, the driving electrode is considered to be connected to a DC voltage, while the sensing electrode is left empty. Based on this, an electric field distribution will be formed in the local region in the testing concrete sample under the electrode pair and the air gap between the sample and probe. This seems to be a reasonable approximation to the situations to be met in capacitive imaging for concrete inspection. The concrete considered in this model is assumed to be a non-magnetic material. As such, the magnetic permeability of concrete is deemed equal to that of free space. In terms of the electrical properties, in practice the permittivity and conductivity will depend on the frequency used to drive the electrodes, the moisture content and the thickness of the concrete material, as well as other factors such as the mix used etc. As the main purpose of the FE modelling here is to demonstrate the possibility of imaging surface and sub-surface features, hidden defects and steel rebars—i.e., we are only interested in demonstrating that the contrast in electrical properties between the various materials (concrete, steel, air/water voids) gives rise to measurable signals—simplifications can be made. Thus, it has been assumed that the permittivity and conductivity of concrete samples can be assumed to have a nominal value, apart from defects or other features that can deviate from this. In addition, these values are assumed to be frequency independent. In the theoretical model, the relative permittivity was set to a value of 6, and the conductivity to 0.02 s m^{-1}, a value used in other published work [37].

The model geometry is shown in Fig. 5. This represents a slab of concrete containing regions of discontinuity in electric properties. The electrodes were modelled at the relative sizes shown in the figure. Note that the field distribution predicted by these models is determined primarily by these geometric factors in the quasi-static model.

Assuming the geometry of Fig. 5, the FE model can be used to predict the equipotential lines within the resultant electric field

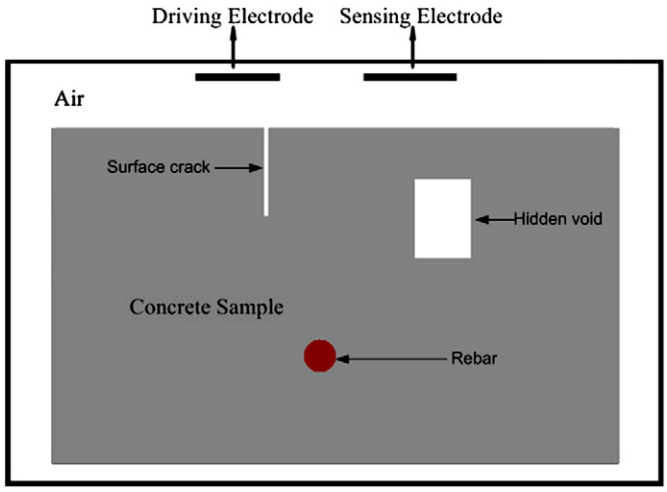

Fig. 5. Model used for FE simulation of CI for concrete sample.

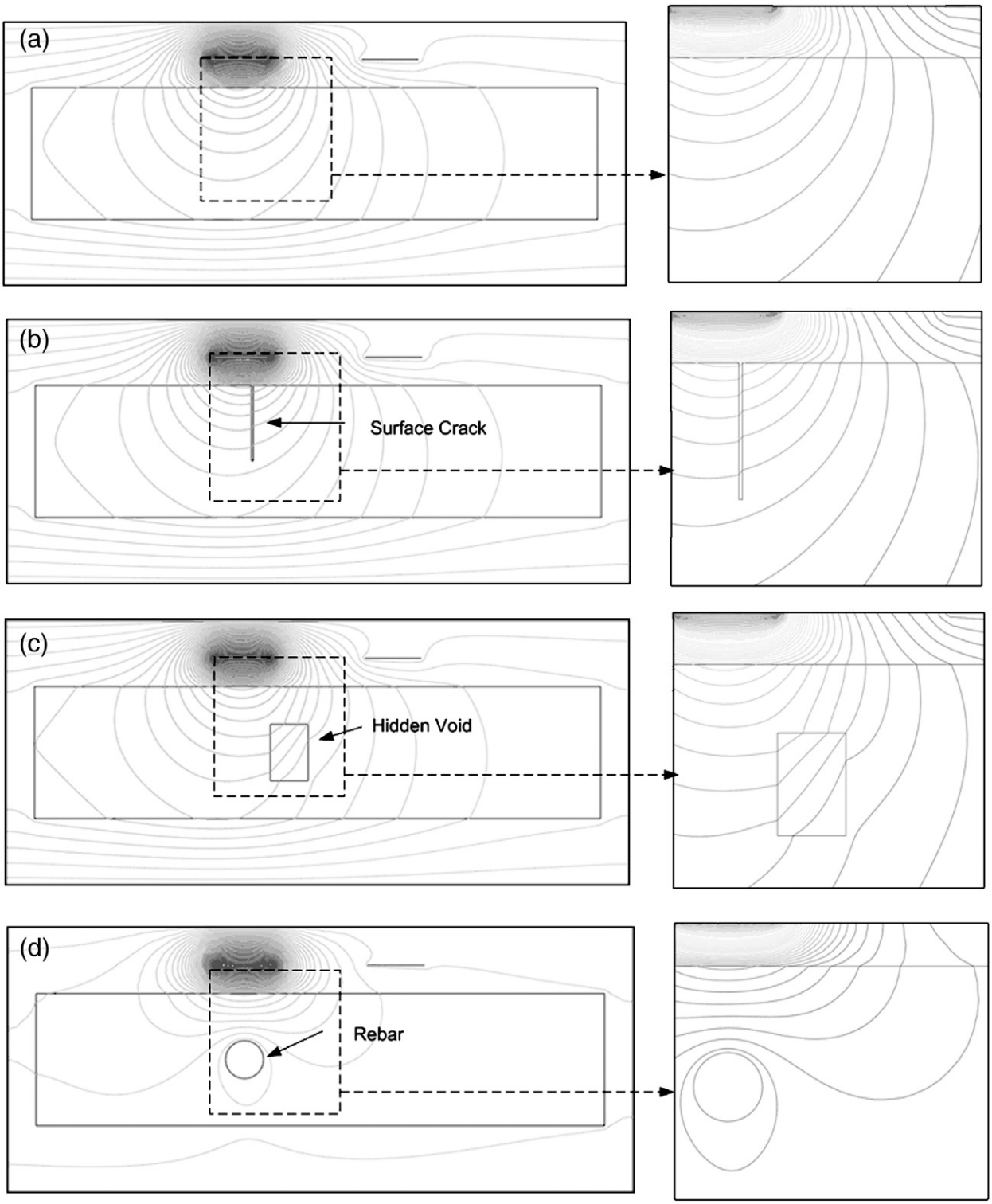

Fig. 6. Simulations of the electric field distribution for a concrete sample. Results are shown for (a) a uniform sample (b) a sample with a narrow crack on the surface, (c) a simulated void under the surface and (d) a steel rebar in the location shown.

distribution. These are shown in Fig. 6 for (a) a uniform concrete sample (b) a sample with a narrow crack on the surface, (c) a simulated void under the surface and (d) a steel rebar in concrete.

The areas in the dashed boxes of each model are expanded to show the distributions of the electric field, and the capacitance recorded by the capacitive probe in each case was calculated and is shown in Table 1.

It can be seen in the later three cases, the electric field distribution becomes distorted within and around the regions of discontinuity in

Table 1
Calculated capacitance value from the FE models.

Model	Calculated Capacitance
Capacitive imaging probe above a complete sample	7.319×10^{-13}(F)
Capacitive imaging probe above a sample with a surface crack	6.998×10^{-13}(F)
Capacitive imaging probe above a sample with a hidden void	7.526×10^{-13}(F)
Capacitive imaging probe above a sample with a rebar	2.427×10^{-13}(F)

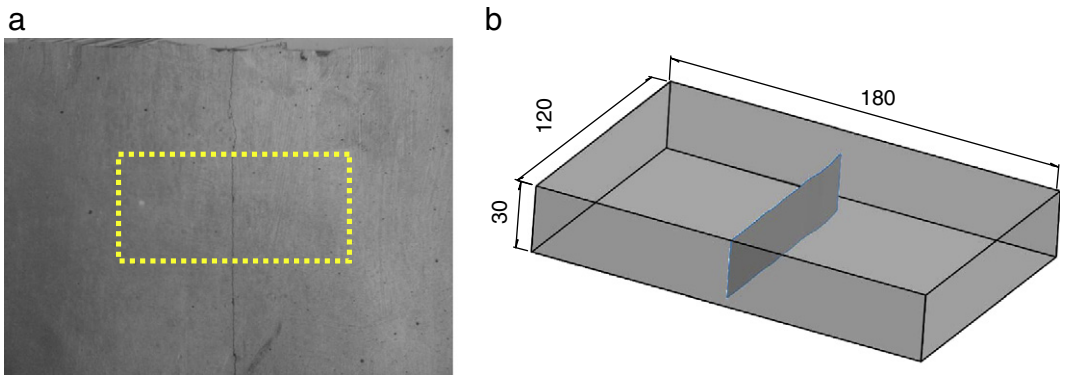

Fig. 7. Concrete specimen with a crack on the surface. (a) Photograph of top surface containing the crack, and (b) schematic diagram of the crack geometry.

the dielectric properties within the sample (i.e. the presence of crack, void or rebar). This is a result of the very different electrical properties of concrete compared to either air or steel. The distorted electric field causes a capacitance change of the capacitive imaging probe, as shown in Table 1, which leads to a detectable signal change on the sensing electrode. This gives some indication that capacitive imaging is capable of forming the basis for a novel NDE system for concrete. This is confirmed by experimental results to be shown later in this paper.

4. Experimental results

The concrete samples used in this work were fabricated from a C40 mix (relative proportions by mass 2.55:1.7:1:0.6 of 20 mm limestone aggregate:sand:CEM1 cement:water) unless otherwise specified. After 28 days of moist curing, the samples were aged for a minimum of 12 months (for small samples) and >2 years (for large samples) in ambient laboratory conditions, so that they could be considered to be reasonably stable in terms of their electrical properties and internal moisture distribution. The apparatus shown in Fig. 4 was used to scan a capacitive electrode pair over the surface of various concrete samples, which had been prepared so as to contain certain features of interest. These included surface cracking, changes in thickness and the presence of rebars.

The first sample that was investigated was a mortar block with dimensions 180 (length)×120 (width)×30 mm (depth), with no coarse aggregate. A surface crack initiated by impact was present on the upper surface, as shown in the photograph of Fig. 7(a). This has been cleaned to show the presence of the crack more clearly.

The electrode assembly shown earlier in Fig. 3 was scanned over a 100 mm×50 mm area, as highlighted by the dotted line in Fig. 7(a), with a 1 mm step size and 1 mm stand-off distance (the gap between the probe and the sample surface). The excitation frequency was 1 MHz. The image resulting from this scan is shown in Fig. 8, where the amplitude of the signal output from the sensing electrode has been plotted against position across the sample surface. It can be seen that there was an obvious discontinuity in the image caused by the presence of the surface crack.

A second concrete specimen with dimensions 980 mm (length)×860 mm (width)×125 mm (depth) was also fabricated, containing a stepped air-filled channel running through the centre to simulate a local change in thickness. The channel had two depth values, 30 mm and 60 mm, so that the cover thickness over the void had values of 125 mm (full sample thickness), 95 mm and 65 mm respectively, as shown in Fig. 9.

The thickness of this sample and the width of the channels meant that a larger pair of electrodes than the 20 mm wide design used in the above measurements and shown earlier in Fig. 3. In this case, the triangular electrodes were each 150 mm wide in the horizontal direction. A scan at a frequency of 1 MHz was performed, over a 540 mm×600 mm area, with a 30 mm step size and 1 mm stand-off distance. The result is shown in Fig. 10. The lighter area indicates the presence of both the shallow void and the deep void, as indicated by the dotted lines which represent the actual positions of the channel. It can also be seen that the shallower channel (with the greater cover depth of 95 mm) produced a lower output than that region containing the smaller cover depth of 65 mm. Hence, it seems that some depth information is available from such scans.

A further set of experiments was now performed, to indicate the presence of rebars. The first test sample, shown in Fig. 11, contained a single 10 mm diameter rebar located at a cover depth of 10 mm.

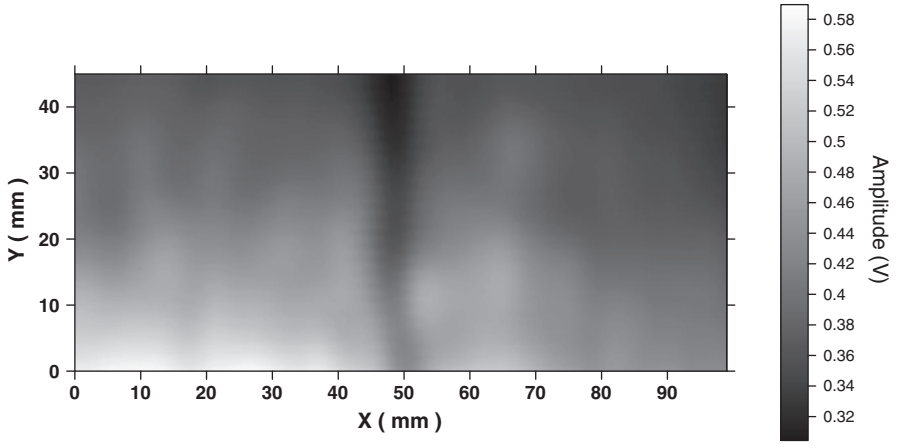

Fig. 8. Capacitive imaging results for concrete sample with a crack on the surface.

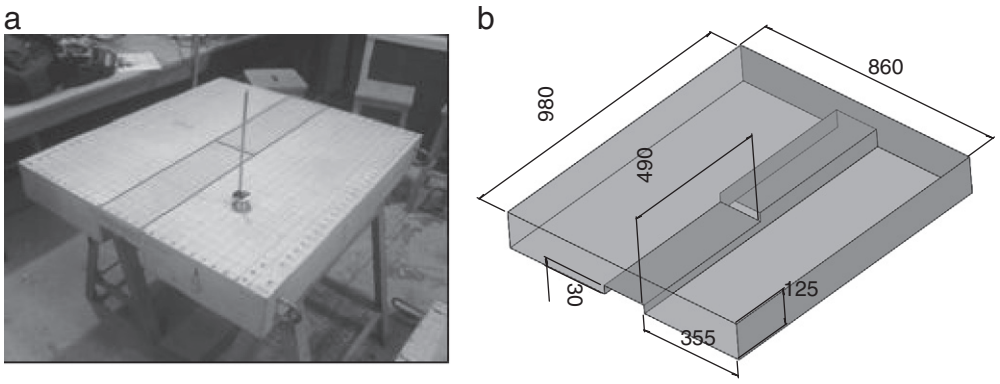

Fig. 9. (a) Photograph and (b) schematic diagram of a concrete sample with a hidden channel of two different depths (30 mm and 60 mm).

The concrete sample itself was of dimensions 300 mm (length) × 150 mm (width) × 30 mm (depth) and in this case, 10 mm aggregate was included in the mix. The rebar was equidistant from the top and bottom surfaces and parallel to them. The rebar and the scanned area are highlighted on the surface of the photograph shown in Fig. 11(a).

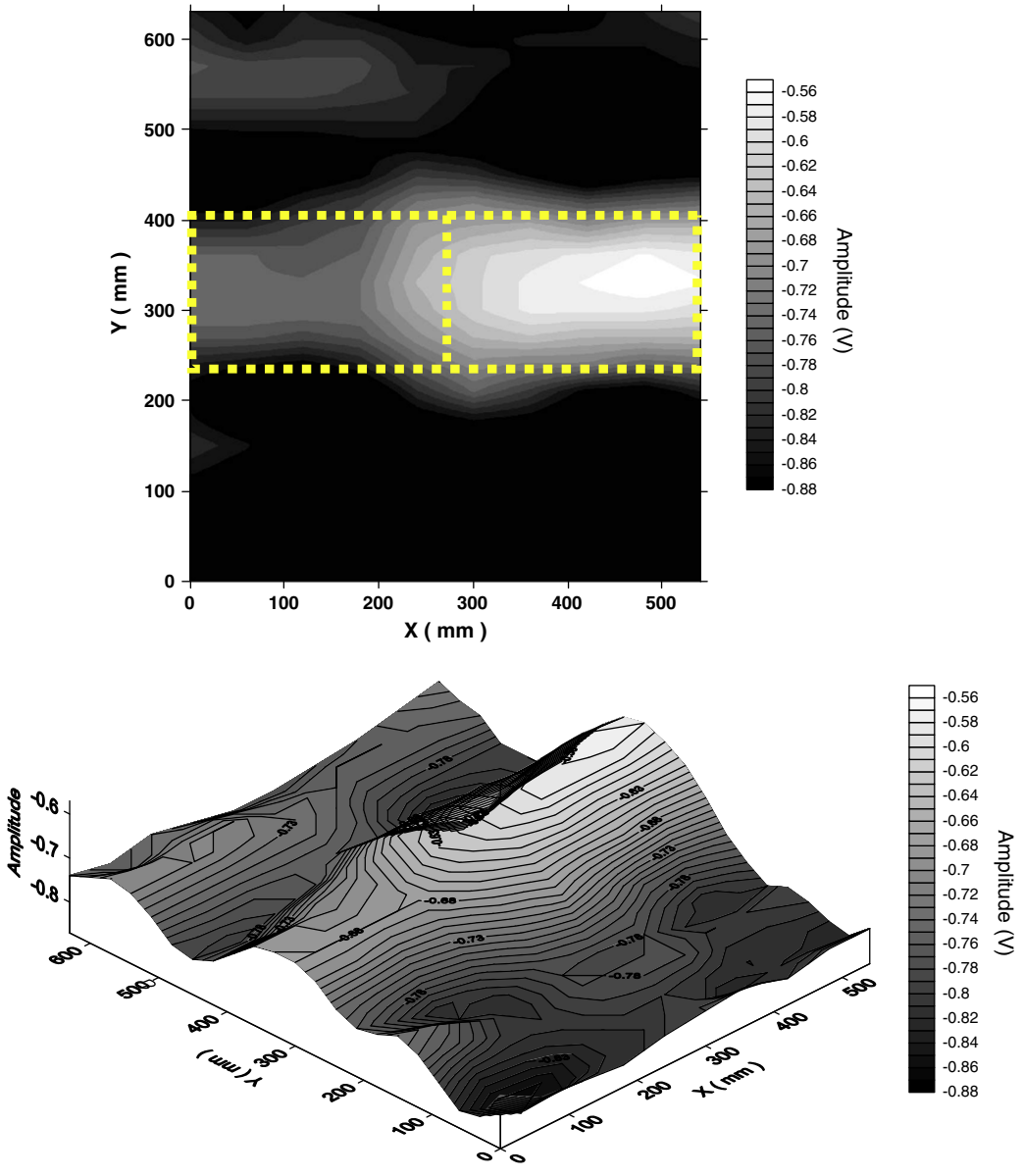

Fig. 10. Capacitive imaging results for concrete sample with hidden stepped channel.

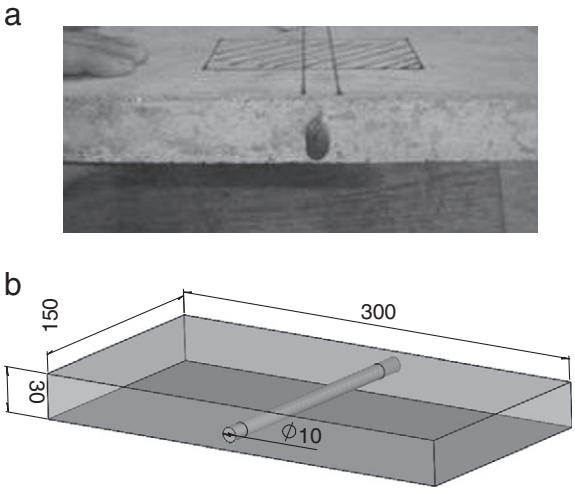

Fig. 11. Concrete sample with a single rebar of 10 mm diameter placed symmetrically within the thickness of a 30 mm thick concrete sample. (a) Photograph of sample, and (b) schematic diagram.

An 80 mm × 60 mm area was scanned using the probe shown in Fig. 3 with a 1 mm step size and a 1 mm stand-off distance, using a 1 MHz driving signal. The resulting image is shown in Fig. 12(a). The rebar can be seen as the darker vertical strip in the centre of the image, which indicates that the capacitive imaging technique was sensitive to the hidden rebar and had detected it successfully. During the scan, the rebar was grounded using a conducting wire with a crocodile clip to enhance the contrast of the image (analogous to similar practice in half-cell potentiometer surveys). Note however that detection of the rebar is also possible with the rebar floating (i.e. not grounded) but the obtained image will have less contrast, as shown in Fig. 12 (b).

A further sample was now prepared containing multiple rebars, and is shown in Fig. 13. It was of 1000 (length) × 1000 (width) × 150 mm (depth), with two sets of rebars of 10 mm diameter passing through the concrete slab and parallel to the top and bottom surfaces. The first set of rebars (two parallel rebars with a 300 mm spacing between their centres) was buried at a depth of 100 mm from the top surface to their centres, and the second set (also two parallel rebars with a 300 mm spacing between the centres), were oriented perpendicular to the first set were buried at a depth of 120 mm from the top surface to their centres. This sample provided a more complex scanning environment, such as that likely to be met in practice, with sets of rebars at different depths and orientation.

A 780 mm × 690 mm area was scanned using the larger probe, using a 1 MHz driving signal. A 30 mm step size and 1 mm stand-off distance were used for the scan, with the rebars again grounded. The result is shown in Fig. 14. The rebars can be seen clearly as the darker areas in the image. Note that the two horizontal features are darker than the two vertical ones; this is because the former represent the two parallel rebars located closest to the scan surface.

5. Discussion of the limitations encountered

It can be seen from the preliminary results that the capacitive imaging technique is sensitive to the presence of surface crack, hidden sub-surface changes in thickness (e.g. voids) and rebars. But due to the co-planar shape of the capacitive imaging probe, which forms a non-linear fringing electric field, there is no analytical formulation to precisely define the measurement volume and penetration depth. This, together with the fact that different kinds of defects could change the local electric properties to the same extent, make the characterization of the crack (width and depth), void (location and size) and rebar (depth and diameter) very difficult by performing one scan using a typical capacitive imaging probe which only has one pair of electrodes. This could be addressed in more advanced systems by using pulsed signals on arrays of multiple electrodes, rather than single pairs, since modelling and experiments in other materials [27] suggests that effective penetration depth is related to electrode spacing. By analysing changes in the relationship between capacitance and electrode spacing caused by artefacts, their depth should be able to be determined.

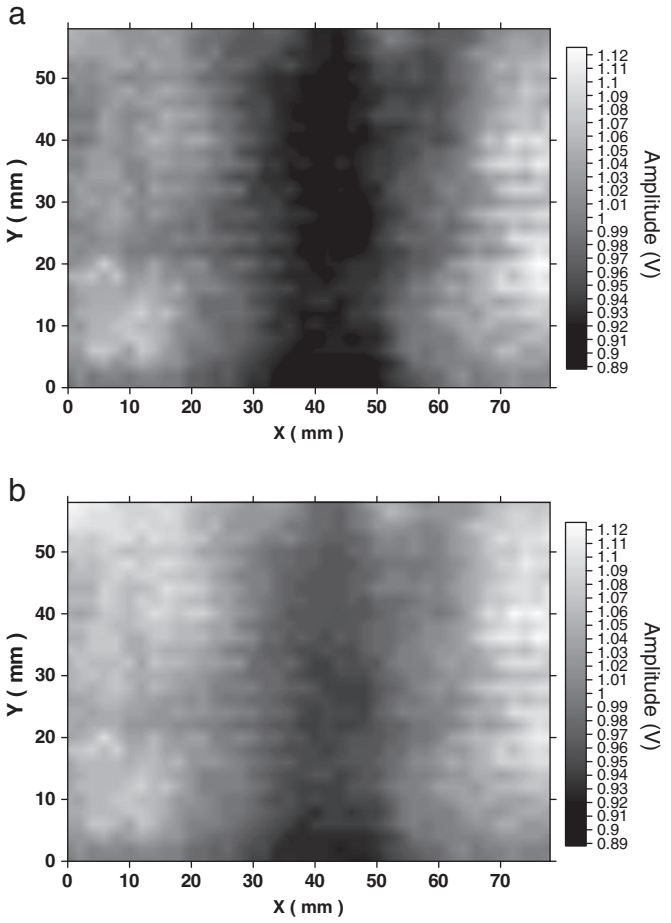

Fig. 12. Capacitive imaging results for the concrete sample of Fig. 9, containing a single rebar. (a) upper figure—electrically grounded rebar. (b) lower figure—electrically ungrounded rebar.

As indicated by the FE models, the electric field lines are denser in the vicinity of the electrode pair, so the capacitive imaging probe is sensitive to the surface features of the concrete specimen and the lift-off distance between the probe and the surface. This sometimes causes confusion in the obtained image, e.g. in Fig. 8 the gradient along the Y-axis in the image is caused by a lack of parallelism between the probe and the sample surface and in Fig. 10, the lighter area on the upper-left part of the image is caused by a pitted area on the surface which may be misinterpreted as a hidden void. More sophisticated signal processing and analysis should be able to distinguish between stray signals caused by such effects and 'real' diagnostic information, perhaps by using the arrays mentioned above combined with multiple frequency interrogative pulses.

6. Conclusions

Previous work [28] has confirmed that the probe size and geometry are the key factors for penetration depth and image resolution

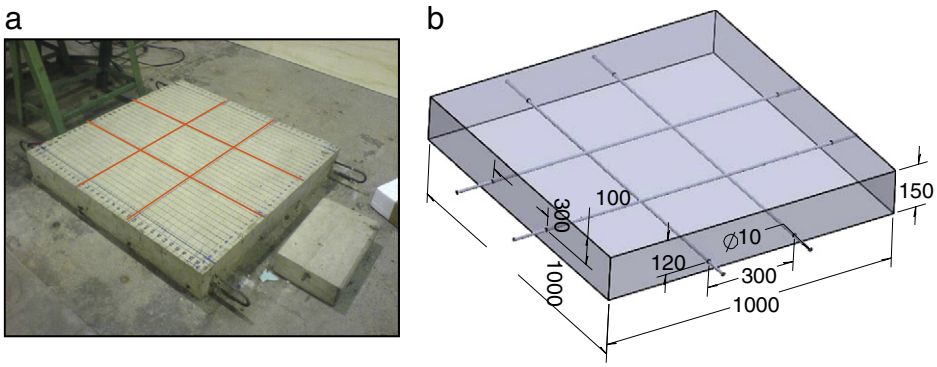

Fig. 13. Concrete sample with rebars (a) photograph of sample, and (b) schematic diagram.

in concrete for the capacitive imaging technique. This is true provided the frequency is kept within a reasonable range (e.g. 10 kHz–1 MHz), so that the quasi-static approximation mentioned in earlier sections is appropriate. This is in contrast to other electromagnetic NDE methods, such as eddy currents and AC potential drop approaches, where the penetration depth and image resolution are heavily dependent on the frequency of the driving signal. Thus, with frequency not being a major factor, the choice of electrode shape and size becomes important. Work reported elsewhere [28] has demonstrated the influence of probe geometry, and has identified the triangular electrodes used here as a good general-purpose design for preliminary tests. However, as a general rule, the use of smaller electrodes will allow a better resolution of near-surface defects, whereas greater penetration comes from larger electrodes for a given electrode geometry. Accordingly, to image the crack on the surface and shallowly buried rebar, a 20 mm wide triangular electrode probe was used in this paper, whereas for imaging deeper features, a 150 mm wide triangular electrode probe was used. The penetration depth can thus be easily modified by using different sizes of either the electrodes and/or the spacing between them. By using a probe array, it should be possible in future work to obtain an image in real time, without the need for mechanical scanning.

The predictions of FE modelling and the results of preliminary experiments both indicate that the capacitive imaging system has the potential to simultaneously detect surface features, changes in thickness to an air void and cover depth and position of rebars in concrete samples. Thus, the technique has the potential to be developed into a single compact device to detect many different features within concrete samples, providing indications of possible defects in concrete samples to guide more comprehensive NDE surveys of a concrete structure is performed by specialised devices. Note that, unlike ultrasound and some other techniques, there is no need for specific surface preparation, and no couplant is required. The technique works in a non-contact and a non-invasive manner, and only requires single-side access to the sample. In addition, the difference in electric properties between details of interest (crack, void and rebar) and concrete is much larger than that between cement paste and aggregate and so the scattering effect encountered in ultrasonic imaging is absent. The transducers are very simple and cheap—effectively, just copper plates—in contrast to complex and expensive piezoelectric or electromagnetic transducers, which means that a wide range of probe geometries and thus assessment applications could be available to practitioners at little added cost.

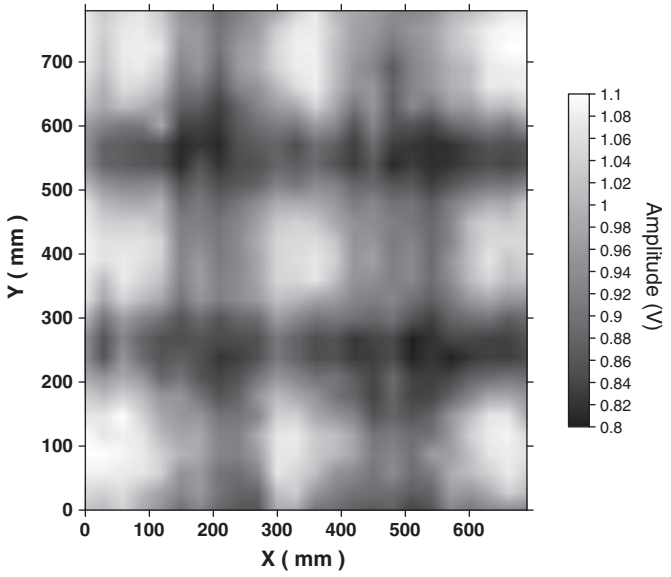

Fig. 14. Capacitive imaging results for the concrete sample shown in Fig. 11.

In practice the situation is usually rather more complicated compared to the samples interrogated in this work. Defect types and sizes will be unknown, moisture conditions may be inhomogenous, and voids may be poorly defined (e.g. by honeycombing). Further development of the capacitive imaging probe is required to meet different practical requirements and provide enhanced diagnostic information, e.g. systematic identification and characterisation of defects. Electrode arrays or multi-electrode probes with flexible combinations of electrode size/shape could help obtain the depth and size information of a sub-surface void/rebar. Advanced signal processing algorithms can filter out stray signals from e.g. changes in surface roughness. Nonetheless, capacitive imaging shows considerable promise for NDE of concrete.

Acknowledgements

The authors would like to acknowledge funding for this research via a Targetted Research Project from the Research Centre for NDE (RCNDE), itself funded partially by the Engineering and Physical Sciences Research Council (EPSRC). Thanks are also due to industrial partners in this research, namely Airbus Industries, BP, Shell and the National Nuclear Laboratory (NNL).

References

[1] S. Rostam, High performance concrete cover—why it is needed, and how to achieve it in practice, Construction and Building Materials 10 (1996) 407–421.
[2] X. Derobert, C. Aubagnac, O. Abraham, Comparison of NDT techniques on a post-tensioned beam before its autopsy, NDT and E International 35 (2002) 541–548.
[3] Ultrasonic tester for concrete, Ultrasonics 9 (1971) 71.
[4] K. Warnemuende, H.-C. Wu, Actively modulated acoustic nondestructive evaluation of concrete, Cement and Concrete Research 34 (2004) 563–570.

[5] P. Antonaci, C.L.E. Bruno, P.G. Bocca, M. Scalerandi, A.S. Gliozzi, Nonlinear ultrasonic evaluation of load effects on discontinuities in concrete, Cement and Concrete Research 40 (2009) 340–346.
[6] M. Saafi, T. Sayyah, Health monitoring of concrete structures strengthened with advanced composite materials using piezoelectric transducers, Composites Part B: Engineering 32 (2001) 333–342.
[7] J.R. Berriman, D.A. Hutchins, A. Neild, T.H. Gan, P. Purnell, The application of time-frequency analysis to the air-coupled ultrasonic testing of concrete, *Ultrasonics, Ferroelectrics and Frequency Control* IEEE Transactions on 53 (2006) 768–776.
[8] P. Purnell, T.H. Gan, D.A. Hutchins, J. Berriman, Noncontact ultrasonic diagnostics in concrete: a preliminary investigation, Cement and Concrete Research 34 (2004) 1185–1188.
[9] M. Schickert, Ultrasonic NDE of concrete, Ultrasonics Symposium Proceedings 1 (2002) 739–748 2002 IEEE, 2002.
[10] S.A. Abo-Qudais, Effect of concrete mixing parameters on propagation of ultrasonic waves, Construction and Building Materials 19 (2005) 257–263.
[11] R.K. Dhir, M.R. Jones, M.J. McCarthy, Quantifying chloride-induced corrosion from half-cell potential, Cement and Concrete Research 23 (1993) 1443–1454.
[12] V. Leelalerkiet, J.-W. Kyung, M. Ohtsu, M. Yokota, Analysis of half-cell potential measurement for corrosion of reinforced concrete, Construction and Building Materials 18 (2004) 155–162.
[13] M. Ohtsu, T. Yamamoto, Compensation procedure for half-cell potential measurement, Construction and Building Materials 11 (1997) 395–402.
[14] S. Ahmad, Reinforcement corrosion in concrete structures, its monitoring and service life prediction—a review, Cement and Concrete Composites 25 (2003) 459–471.
[15] G. Klysz, J.P. Balayssac, Determination of volumetric water content of concrete using ground-penetrating radar, Cement and Concrete Research 37 (2007) 1164–1171.
[16] W.L. Lai, S.C. Kou, W.F. Tsang, C.S. Poon, Characterization of concrete properties from dielectric properties using ground penetrating radar, Cement and Concrete Research 39 (2009) 687–695.
[17] V. Barrile, R. Pucinotti, Application of radar technology to reinforced concrete structures: a case study, NDT & E International 38 (2005) 596–604.
[18] J.H. Bungey, Sub-surface radar testing of concrete: a review, Construction and Building Materials 18 (2004) 1–8.
[19] D.-M. Bontea, D.D.L. Chung, G.C. Lee, Damage in carbon fiber-reinforced concrete, monitored by electrical resistance measurement, Cement and Concrete Research 30 (2000) 651–659.
[20] J.F. Lataste, C. Sirieix, D. Breysse, M. Frappa, Electrical resistivity measurement applied to cracking assessment on reinforced concrete structures in civil engineering, NDT & E International 36 (2003) 383–394.
[21] N. Ozyurt, T.O. Mason, S.P. Shah, Non-destructive monitoring of fiber orientation using AC-IS: an industrial-scale application, Cement and Concrete Research 36 (2006) 1653–1660.
[22] K. Karhunen, A. Seppanen, A. Lehikoinen, P.J.M. Monteiro, J.P. Kaipio, Electrical resistance tomography imaging of concrete, Cement and Concrete Research 40 (2009) 137–145.
[23] P. Purnell, G.G. Diamond, D.A. Hutchins, T.H. Gan, K.K. Leong, Capacitive internal imaging technique for concrete, Abstracts: Cement and Concrete Science (2005) 41–44 15-16th September.
[24] X. Derobert, J. Iaquinta, G. Klysz, J.-P. Balayssac, Use of capacitive and GPR techniques for the non-destructive evaluation of cover concrete, NDT & E International 41 (2008) 44–52.
[25] A.A. Nassr, W.H. Ahmed, W.W. El-Dakhakhni, Coplanar capacitance sensors for detecting water intrusion in composite structures, Measurement Science and Technology 19 (2008) 075702.
[26] A.A. Nassr, W.W. El-Dakhakhni, Non-destructive evaluation of laminated composite plates using dielectrometry sensors, Smart Materials and Structures 18 (2009) 055014.
[27] G.G. Diamond, D.A. Hutchins, T.H. Gan, P. Purnell, K.K. Leong, Single-sided capacitive imaging for NDT, BINDT Insigh 48 (2006) 724–730.
[28] X. Yin, G.G. Diamond, D.A. Hutchins, Further invesitigations into capacitive imaging for NDE, BINDT insight 51 (2009) 484–490.
[29] O. Vendik, S. Zubko, M. Nikol'skii, Modeling and calculation of the capacitance of a planar capacitor containing a ferroelectric thin film, Technical Physics 44 (1999) 349–355.
[30] G. Meng, A.J. Jaworski, J.C.S. Kimber, A multi-electrode capacitance probe for phase detection in oil-water separation processes: design, modelling and validation, Measurement Science and Technology 17 (2006) 881–894.
[31] A.J. Jaworski, G.T. Bolton, The design of an electrical capacitance tomography sensor for use with media of high dielectric permittivity, Measurement Science and Technology 11 (2000) 743–757.
[32] F. Jiang, S. Liu, J. Liu, X. Wang, Measurement of ice movement in water using electrical capacitance tomography, Journal of Thermal Science 18 (2009) 8–12.
[33] R. Nimmer, J. Osiensky, A. Binley, K. Sprenke, B. Williams, Electrical resistivity imaging of conductive plume dilution in fractured rock, Hydrogeology Journal 15 (2007) 877–890.
[34] G.M. Maillet, E. Rizzo, A. Revil, C. Vella, High resolution electrical resistivity tomography (ERT) in a transition zone environment: application for detailed internal architecture and infilling processes study of a Rhône River Paleo-channel, Marine Geophysical Researches 26 (2005) 317–328.
[35] V. Spitas, P. Michelis, The potential drop technique for measuring crack growth in shear, in Fracture of Nano and Engineering Materials and Structures (2006) 463–464.
[36] M. Saka, M. Nakayama, T. Kaneko, H. Abé, Measurement of stress-intensity factor by means of a-c potential drop technique, Experimental Mechanics 31 (1991) 209–212.
[37] J. Davis, Y. Huang, S.G. Millard, J.H. Bungey, "Determination of dielectric properties of insitu concrete at radar frequencies," in International Symposium, DGZfP, Berlin Germany, 2003.